

Tetragonal CuMnAs alloy: role of defects

F. Máca^a, J. Kudrnovský^a, P. Baláž^{b,c}, V. Drchal^a, K. Carva^b, I. Turek^b

^a*Institute of Physics ASCR, Na Slovance 2, CZ-182 21 Praha 8, Czech Republic*

^b*Charles University, Faculty of Mathematics and Physics, Department of Condensed Matter Physics, Ke Karlovu 5, CZ-121 16 Praha 2, Czech Republic*

^c*IT4Innovations Center, VSB Technical University of Ostrava, 17. listopadu 15, CZ-708 33 Ostrava-Poruba, Czech Republic*

Abstract

The antiferromagnetic (AFM) CuMnAs alloy with tetragonal structure is a promising material for the AFM spintronics. The resistivity measurements indicate the presence of defects about whose types and concentrations is more speculated as known. We confirmed vacancies on Mn or Cu sublattices and Mn_{Cu} and Cu_{Mn} antisites as most probable defects in CuMnAs by our new ab initio total energy calculations. We have estimated resistivities of possible defect types as well as resistivities of samples for which the X-ray structural analysis is available. In the latter case we have found that samples with Cu- and Mn-vacancies with low formation energies have also resistivities which agree well with the experiment. Finally, we have also calculated exchange interactions and estimated the Néel temperatures by using the Monte Carlo approach. A good agreement with experiment was obtained.

Keywords: antiferromagnetics, defects, transport, ab initio calculations, Monte Carlo simulations

PACS: 75.25.+z, 75.30.Et, 75.47.Np, 75.50.Ee

1. Introduction

The CuMnAs crystallizes in the orthorhombic phase [1], the tetragonal phase can be prepared only under special conditions by separation from an ingot or as a film by the molecular beam epitaxy (MBE) on a suitable substrate, namely GaAs(001) and GaP(001) [2]. The tetragonal antiferromagnetic (AFM) CuMnAs phase has attracted recently large interest as promising material for applications in the so-called AFM spintronics [2, 3, 4, 5].

The first experiments [4, 6] found basic characteristics including structural parameters that were used in first-principles calculations assuming an ideal structure without defects [4]. The experiment on real samples gave the residual resistivity around $90 \mu\Omega\text{cm}$ for low temperature $T \approx 5 \text{ K}$ and $160 \mu\Omega\text{cm}$ for room temperatures [4]. The measurements indicate local Mn moments around $3.6 \mu_{\text{B}}$ at room temperature [4], the Néel temperature around 480 K has been found [7].

The residual resistivity indicates the presence of defects whose origin and concentrations are known only very approximately [6]. Our previous study [8] identified the most probable defects but the evaluation of their formation energies represents a challenge for the theory. The same concerns also an estimate of the residual resistivity and the Néel temperature.

In this contribution we will present a more accurate estimate of formation energies and discuss in detail resistivities of samples for which possible defect structures were

obtained by the X-ray analysis. Finally, we also present new, more accurate estimates of the Néel temperature for both ideal samples and samples containing Mn_{Cu} -antisites.

2. Formalism

The AFM-CuMnAs prepared by the MBE has a tetragonal structure [4, 6] with the space group P4/nmm (No. 129) [9]. The atomic basis contains two formula units (6 atoms), Cu atoms are in the basal plane of the tetragonal lattice, (Wyckoff position $2a$), there are two parallel layers of As atoms (Wyckoff position $2c$) and two layers of Mn atoms (Wyckoff position $2c$) with oppositely oriented moments. The experimental lattice parameters are $a=b=3.82 \text{ \AA}$ and $c=6.318 \text{ \AA}$. The relative positions of atoms (in units of c) are $z_{\text{Cu}}=0.0$, $z_{\text{Mn}}=0.330$, and $z_{\text{As}}=0.266$.

This geometry is used in the VASP calculations (Vienna ab initio simulation package using the projector augmented wave scheme [10]) with the GGA exchange correlation potential [11] to evaluate formation energies of defects. The supercell of 96 atoms simulates the sample with defects. For VASP calculations we have used $E_{\text{cut}} = 300 \text{ eV}$, Brillouin zone sampling with 343 special k-points in the irreducible three-dimensional wedge of ideal tetragonal CuMnAs structure and correspondingly larger number of k-points in the supercells of lower symmetry including defects. We used atomic force minimization to relax the positions of individual atoms in systems with defects.

The transport coefficients and exchange interactions applied in evaluation of resistivity and the Néel temperature are determined using the Green function formulation

Email address: maca@fzu.cz (F. Máca)

of the tight-binding linear muffin-tin orbital (TB-LMTO) method in which the effect of disorder (defects) is described by the coherent potential approximation (CPA) [12]. We have verified a good agreement between densities of states of ideal CuMnAs and alloy with Mn_{Cu}-antisites obtained both by the supercell VASP and TB-LMTO-CPA calculations [8] used below to estimate the transport properties and exchange interactions.

The transport studies employ the Kubo-Greenwood linear response theory in which the disorder-induced vertex-corrections are included in the CPA [13]. The effective exchange interactions between Mn atoms for a given shell s , J_s , are determined by the Lichtenstein mapping procedure [14] generalized to random alloys [15]. Specifically, the disordered local moment (DLM) or paramagnetic reference state [8] was used.

To study the thermodynamic properties of CuMnAs we employed classical Monte Carlo (MC) simulations based on the Metropolis algorithm [16]. For simulations we used a 3-dimensional supercell composed of up to $24 \times 24 \times 24$ elementary CuMnAs cells with periodic boundary conditions.

3. Results and discussion

3.1. Formation energies of defects in AFM-CuMnAs

In previous study [8] we have determined formation energy of defects assuming a single impurity in the supercell. This procedure leads to finite supercell magnetic moments for defects including Mn-atoms. In the present study we have repeated calculations by assuming two Mn-atoms with opposite magnetic moments in the supercell to warrant its total zero magnetic moment (the supercell size is thus two times larger for the same defect concentration). The calculated total energy in this model, contrary to previous single impurity one, depends on relative positions of defects. We have chosen the most distant position allowed by the supercell size. Specifically, we have employed 96 atoms to simulate 6.25% defect concentrations. While the lattice parameters (a , c) given by experiment were kept fixed in all cases we have optimized atomic positions inside the supercell (relaxed system). The accurate determination of formation energies (FE) is a challenging task (see, e.g., a recent review [17]). To identify the most probable defects we employ the simple approach in which the FE is defined as $FE = E_{\text{tot}}[\text{def}] - E_{\text{tot}}[\text{id}] - \sum_i n_i E_i$, where $E_{\text{tot}}[\text{def}]$ and $E_{\text{tot}}[\text{id}]$ are total energies of the supercells with (def) and without (id) defects, n_i indicates the number of atoms of type i ($i = \text{Cu, Mn, As, vacancy}$) that have been added to ($n_i > 0$) or removed from ($n_i < 0$) the supercell when the defect is formed, and E_i are total energies of atoms in their most probable bulk phase [17]. It should be noted that actual values for the FE depend on the choice of these energies and on the determination of $E_{\text{tot}}[\text{def}]$. Results for most common defects are given in Table 1.

Table 1: The formation energies FE for various substitutional defects in the tetragonal antiferromagnetic CuMnAs. The symbol XY denotes the X-defect on the Y-sublattice.

Defect	FE [eV]	Defect	FE [eV]
Vac _{Mn}	-0.16	As _{Cu}	+1.73
Vac _{Cu}	-0.14	As _{Mn}	+1.79
Mn _{Cu}	-0.03	Mn _{As}	+1.92
Cu _{Mn}	+0.34	Vac _{As}	+2.18
Cu _{As}	+1.15		

The results show only small shift of FE if the antiferromagnetic elementary cell was used instead of a magnetic one. The same qualitative results have been obtained: vacancies on Mn- and Cu-sublattices (Vac_{Mn}, Vac_{Cu}) and Mn_{Cu} and Cu_{Mn} are the most probable defects. Mn-interstitials, Mn_{As} or As_{Mn} and related defects have large FE. Nevertheless, we note that FE's of defects depend on delicate details of the impurity kinetics which is not considered here. We suppose that defects with low FE's are more probable candidates than those with larger FE's even at the non-equilibrium conditions.

We note that the quality of samples prepared by MBE is strongly affected by the substrate used for growth of the tetragonal CuMnAs film. This complicates the comparison of theoretical results with results of X-ray analysis of real samples. High concentrations of Cu_{As} and Mn_{As} antisites, defects with larger formation energies have been found [6] for samples grown on GaAs, material with a large mismatch of lattice constants to CuMnAs.

3.2. Transport properties of AFM-CuMnAs

In the previous section we have estimated formation energies of possible defects in the tetragonal CuMnAs. The primary aim was to indicate the defects responsible for a finite (planar) resistivity ($\rho_{\text{pl}} = \rho_{xx} = \rho_{yy}$) observed in the experiment. Here we adopt an alternative strategy and estimate the resistivities of defects listed in Table 1 assuming acceptable defect concentrations of five percent on each of equivalent sublattices to determine a suitable defect responsible for a finite sample resistivity. We have calculated the planar resistivities for each defect-type listed in Table 1 including also the Cu \leftrightarrow Mn swap defect. In some cases (see Table 3) we will also present calculated values of the resistivity normal to the planar one (ρ_{zz}) and the total resistivity ($\rho_{\text{tot}} = (2 \rho_{\text{pl}} + \rho_{zz})/3$). The experimental planar resistivity at very low temperature is about $90 \mu\Omega\text{cm}$.

The results are summarized in Table 2 with the following conclusions: (i) The defects with low formations energies (Vac_{Mn}, Vac_{Cu}, Mn_{Cu}, and Cu_{Mn}) generally give small planar resistivities as compared to the experiment. The exception is Mn_{Cu}-antisite with a pronounced virtual bound state at the Fermi energy [8] which results in larger resistivity; (ii) There are relatively large resistivities for

Table 2: Calculated planar resistivities ρ_{pl} (in $\mu\Omega\text{cm}$) for the tetragonal CuMnAs assuming 5% of different defect types on each of equivalent sublattices. Defect types are the same as those listed in Table 1 with the exception of the Cu \leftrightarrow Mn swaps.

Model	ρ_{pl}	Model	ρ_{pl}
Vac _{Cu}	12	As _{Cu}	94
Vac _{Mn}	36	As _{Mn}	113
Mn _{Cu}	111	Vac _{As}	174
Cu _{Mn}	24	Mn _{As}	122
Cu _{As}	107	Mn \leftrightarrow Cu swap	124

defects on the As-sublattice (Cu_{As}, Vac_{As}, and Mn_{As}). These large resistivities correspond to defects with high formation energies; and (iii) It is interesting to note that the sum of resistivities of Mn_{Cu} and Cu_{Mn} ($135 \mu\Omega\text{cm}$) is comparable to the resistivity of Cu \leftrightarrow Mn swap ($124 \mu\Omega\text{cm}$).

In real conditions which are far from the thermodynamical equilibrium and with possible violation of the sample stoichiometry, the resistivities depend on the actual occupation of sublattices by the alloy constituents resulting in the presence of antisite sublattice disorder. This is a challenging problem for the structural X-ray analysis in the present alloy because of similar scattering cross sections of atoms forming the alloy (Cu and Mn). We have found two such attempts, namely Refs. [6] and [18], referred below as models I and II, respectively. The first model I [6], simulating a sample grown on GaAs substrate and schematically written as Cu-(Mn_{0.86},Vac_{0.14})-(As_{0.84},Cu_{0.08},Mn_{0.08}), assumes a small Cu-excess (fully occupied Cu-sublattices with Cu_{As} antisites), and, at the same time, a reduced Mn-content with Mn-vacancies on Mn-sublattice (Vac_{Mn}) and some Mn_{As} antisites. While Mn-vacancies have favorable formation energies, the Cu_{As} antisite and, in particular, Mn_{As} ones have large formation energies (see Table 1). We have also tested a model Ia with halved defect concentrations. The other model II [18], simulating a sample grown on GaP substrate and schematically written as (Cu_{1-x},Vac_x)-(Mn_{1-y},Vac_y)-As has fully occupied As-sublattice and vacancies on Cu- and Mn-sublattices with very favorable formation energies. A detailed analysis [18] has led to two possible structural realizations, namely model IIa ($x=11\%$ and $y=4\%$) and model IIb ($x=18\%$ and $y=8\%$). We have also tested a theoretical choice of x and y in the spirit of the model II, namely the model IIc with $x=y=10\%$. According to [2] the samples grown on GaAs are of significantly worse structural quality as compared to the samples grown on GaP. The available resistivity data are for the GaP samples.

Results are summarized in Table 3 with the following conclusions: (i) In general, resistivities in the direction normal to the plane (ρ_{zz}) are larger as compared to the planar ones and so it is also for the total resistivity ρ_{tot} ;

Table 3: The calculated resistivities ρ_{pl} , ρ_{zz} and ρ_{tot} (in $\mu\Omega\text{cm}$) for models obtained from the X-ray structural analysis, namely models I, Ia, IIa, IIb, and IIc (see text for details). We also show resistivities of separate defects.

	Model	ρ_{pl}	ρ_{zz}	ρ_{tot}
I	14% Vac _{Mn} 8% Cu _{As} 8% Mn _{As}	179	213	282
Ia	7% Vac _{Mn} 4% Cu _{As} 4% Mn _{As}	148	200	304
	8% Mn _{As}	141	202	324
	8% Cu _{As}	129	190	311
	14% Vac _{Mn}	95	138	225
IIa	11% Vac _{Cu} 4% Vac _{Mn}	49	171	90
IIb	18% Vac _{Cu} 8% Vac _{Mn}	89	163	113
IIc	10% Vac _{Cu} 10% Vac _{Mn}	89	182	120

(ii) Models of the II-type with Cu- and Mn-vacancies are compatible with estimated low formation energies (see Table 1); (iii) The experimental determination of exact vacancy concentrations is not an easy task. The lower planar resistivity of the model IIa in comparison with the model IIb is related to a very small resistivity due to Cu-vacancies as compared to that due to Mn-vacancies (3 times lower, see Table 2). The explanation is not so easy as different vacancies also mean differently reduced number of carriers (different valency of Cu- and Mn-atoms). Nevertheless, both models IIb and IIc agree very well with the measured planar resistivity at the very low temperature (about $90 \mu\Omega\text{cm}$); (iv) On the other hand, the model I with relatively high concentrations of Cu_{As} and Mn_{As} antisites with high formation energies (see Table 1) gives a large planar resistivity, even with a halved defect concentrations (model Ia). As it is seen from the Table 2 both defects have separately large planar resistivities. It should be noted, however, that for the model I grown on the GaAs substrate are no available transport data; and (v) For model I we have also compared its resistivity with the sum of resistivities of separate defects, i.e., with cases of Cu_{As}- and Mn_{As}-antisites (each with defect concentrations of 8%) and the case of 14% of Mn-vacancies. Their sum ($365 \mu\Omega\text{cm}$) is two times larger. Such difference has to be ascribed to different carrier concentrations in the model I and those in separated cases. In different words, while on one side is the list of resistivity patterns (Table 2) useful for a qualitative discussion, it cannot be taken literally for realistic alloys with complex defect occupations of sublattices with varying carrier concentrations.

We will now discuss a possible effect of temperature on the transport. In addition to the contribution from defects, also phonons (lattice displacements due to finite temperature) and the spin-disorder (spin deviations due to temperature) contribute. A full discussion is beyond the scope of this paper, in addition such studies are limited to simple

lattices [19, 20]. We present results of two simple models, namely the so-called spin-disorder resistivity (SDR) or the resistivity of the paramagnetic state above the Néel temperature, and the spin-independent finite-relaxation time (FRT) model which can serve as a qualitative model for the effect of phonons. The SDR is simulated by the DLM [21, 22] which is a proper description of the paramagnetic state while the FRT model is realized by adding a finite imaginary part $\text{Im } z$ to the Fermi energy in Green functions entering the Kubo-Greenwood formula. The FRT model has no relations to specific temperature while the SDR corresponds to the largest possible spin-disorder at the Néel temperature. The contribution of spin fluctuations well below the Néel temperature is much smaller as compared to the SDR.

The calculated planar SDR's of the ideal CuMnAs sample as well as of samples with Mn_{Cu} -antisites and $\text{Cu} \leftrightarrow \text{Mn}$ swaps (5%) are in the range of 225 to 235 $\mu\Omega\text{cm}$ indicating a weak influence of chemical disorder. The SDR is thus larger than the experimental planar resistivity at the room temperature (300 K, 150 $\mu\Omega\text{cm}$). This could be expected because the Néel temperature lies well above the room temperature. The spin disorder at room temperature is then rather weak.

We have also calculated resistivity of the model IIc in the framework of the FRT model for two choices of $\text{Im } z$, namely, $\text{Im } z = 2$ mRy and 5 mRy, respectively. Calculated planar resistivities are 113 and 143 $\mu\Omega\text{cm}$, respectively and they are compatible with the experimental data at the room temperature assuming some unspecified contribution due to spin-disorder.

3.3. Exchange interactions and the Néel temperature

The exchange interactions were estimated from the paramagnetic reference state described by the DLM model. It describes the finite critical temperature more naturally than the state at zero temperature (the AFM reference state). In addition, the paramagnetic state assumes no magnetic order and the only non-zero interactions are those among Mn-atoms. We have demonstrated earlier [8] that for well localized moments like Mn-ones in CuMnAs, both approaches give similar although not identical values of exchange integrals. We have obtained strongly dominating AFM interactions even from the DLM reference state which are a precursor of the AFM ground state below the Néel temperature. Calculated exchange interactions were used to construct the effective classical Heisenberg Hamiltonian from which the Néel temperature was estimated by applying the MC simulations. Specifically, we have employed the atomistic spin dynamics (ASD) codes [23]. For ideal CuMnAs alloy as well as for systems with vacancies only Mn atoms on their native sublattices are considered in MC simulations while for Mn_{Cu} antisites on Cu sublattice we consider also interactions between antisite Mn-atoms as well as interactions between antisite and native Mn-atoms. The magnetic moments on Mn atoms and the exchange interactions between Mn atoms in the supercell were set

utilizing the results of the *ab initio* calculations. The local Mn magnetic moments were assumed to be independent of temperature. To estimate the average magnetization of the sample and its higher statistical moments we made use of classical MC method based on the Metropolis algorithm.

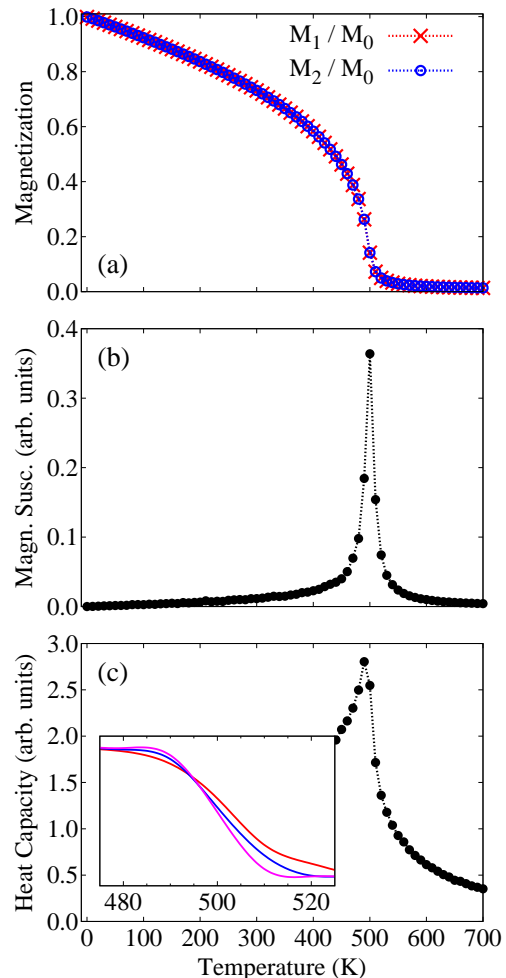


Figure 1: (a) Relative magnetizations of the Mn sublattices as a function of temperature assuming exchange interactions derived from the paramagnetic (DLM) state of the ideal tetragonal CuMnAs. (b) The magnetic susceptibility as a function of the temperature for such CuMnAs alloy. (c) The temperature dependence of the heat capacity for this system. In the inset we show the Binder cumulants for $N = 16, 20, \text{ and } 24$ as a function of the temperature. The Néel temperature corresponds to a common intersection of all three curves (495 K).

Results of the MC simulation for ideal tetragonal CuMnAs alloy are shown in Fig. 1. In Fig. 1(a) we plot magnetizations of the native Mn sublattices as a function of the temperature. As the temperature increases the sublattice magnetizations are reduced due to spin fluctuations and become zero above the critical Néel temperature T_N . The linear decrease of magnetization at low temperatures is a consequence of the use of the classical statistics. Recently a way how to include the quantum statistics into MC simulations has been suggested [24].

The Néel temperature has been estimated from: (i) The peak in the magnetic susceptibility [see Fig. 1(b)]; (ii) the peak in the heat capacity [see Fig. 1(c)], and (iii) the intersection of the Binder cumulants [25] [see inset of Fig. 1(c)]. The estimate (iii) is considered to be the most accurate estimate of the Néel temperature. All methods lead to similar results for the Néel temperature, namely $T_N = 495$ K.

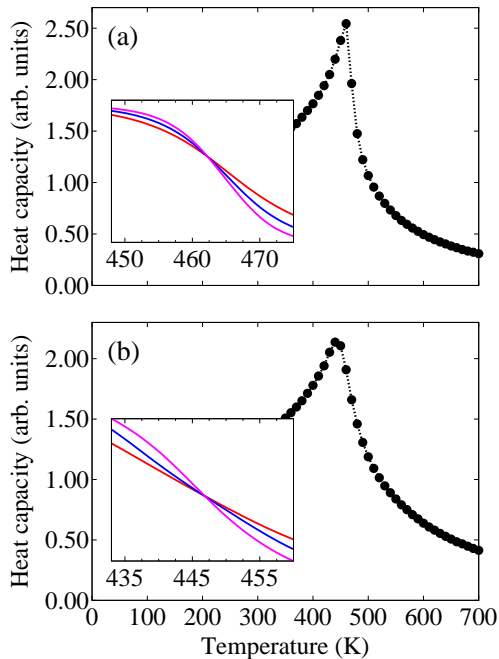


Figure 2: The temperature dependence of the heat capacity derived from the paramagnetic (DLM) state of the disordered tetragonal CuMnAs alloy: (a) with Mn_{Cu} -antisites (5%) and (b) with vacancies on Cu and Mn (model IIa - see text). In the insets are shown corresponding Binder cumulants for $N = 16, 20,$ and 24 as a function of the temperature. The Néel temperature of 465 K and 446 K has been found.

We have also studied two alloys in which defects are present, namely the case of Mn_{Cu} antisites and model IIa containing vacancies on Mn- and Cu-sites [18]. The latter case is simpler, as we have again only exchange interactions among Mn-atoms of the native Mn-sublattice, which contains vacancies, i.e., Mn atoms are now randomly distributed among Mn lattice sites.

For Mn_{Cu} defects the situation is more complicated. The supercell is composed of both native Mn atoms organized in two equivalent fully occupied sublattices and of Mn_{Cu} dopants distributed randomly on two equivalent Cu-sublattices.

Randomly distributed Mn atoms were modeled by 10 independent superlattices with the same amount of Mn atoms. The superlattices differ by distribution of Mn atoms. The simulation started from an initial temperature 900 K which decreased by $\Delta T = 10$ K. At each temperature 4×10^5 MC steps were performed. To improve the statis-

tics, for each of the 10 configurations of Mn_{Cu} defects we simultaneously simulated 5 independent identical systems. The final results were obtained by averaging through all Mn_{Cu} configurations.

The presence of disorder decreased the Néel temperature. The results are shown in Fig. 2 for estimates based on the specific heat and Binder cumulants, respectively. The calculated T_N obtained from Binder cumulants are 465 K and 446 K for the case with 5% of Mn_{Cu} -antisites and for the model IIa, respectively.

4. Conclusions

We have performed an extensive ab initio study of electronic, magnetic, and transport properties of the tetragonal AFM-CuMnAs alloy with potential technological applications. The VASP approach was used for the estimate of formation energies of possible defects while the TB-LMTO-CPA method was used to calculate transport properties and exchange integrals. Finally, the Néel temperatures were determined using the Monte-Carlo approach from calculated exchange integrals. The main conclusions are: (i) The vacancies on Mn- and Cu- sublattices, and Mn_{Cu} and Cu_{Mn} antisites have the lowest formation energies and can be considered as possible candidates for defects in CuMnAs; (ii) These predictions are in a good agreement with the X-ray structural analysis of samples grown on GaP(001) substrate, in addition, the samples with Cu- and Mn-vacancies have also the resistivity close to that found in the experiment; and (iii) We have also obtained a good agreement between experimental and calculated Néel temperatures. Specifically, the vacancies on Mn and Cu as well as the antisite Mn_{Cu} defects reduce the calculated Néel temperature in comparison with that for the ideal CuMnAs while keeping a good agreement with experiment for both quantities.

Acknowledgements

We gratefully acknowledge discussions with C. Frontera about the problems of experimental determination of CuMnAs sample compositions. We acknowledge the financial support from the Czech Science Foundation (Grant No. 14-37427G). This work was supported by The Ministry of Education, Youth and Sports - project IT4Innovations National Supercomputing Center LM2015070 and by the National Grid Infrastructure MetaCentrum - project LM2015042.

References

- [1] F. Máca, J. Mašek, O. Stelmakhovych, X. Marti, K. Uhlířová, P. Beran, H. Reichlová, P. Wadley, V. Novák, and T. Jungwirth, Room-temperature antiferromagnetism in CuMnAs, *J. Magn. Mater.* 324 (2012) 1606.

- [2] P. Wadley, B. Howells, J. Železný, C. Andrews, V. Hills, R.P. Champion, V. Novák, K. Olejník, F. Maccherozzi, S.S. Dhesi, S.Y. Martin, T. Wagner, J. Wunderlich, F. Freimuth, Y. Mokrousov, J. Kuneš, J.S. Chauhan, M.J. Grzybowski, A.W. Rushforth, K.W. Edmonds, B.L. Gallagher, and T. Jungwirth, Electrical switching of an antiferromagnet, *Science* 351, (2016) 587.
- [3] T. Jungwirth, X. Marti, P. Wadley, and J. Wunderlich, Antiferromagnetic spintronics, *Nat. Nanotech.* 11 (2016) 231.
- [4] P. Wadley, V. Novák, R.P. Champion, C. Rinaldi, X. Martí, H. Reichlová, J. Železný, J. Gazquez, M.A. Roldan, M. Varela, D. Khalyavin, S. Langridge, D. Kriegner, F. Máca, J. Mašek, R. Bertacco, V. Holý, A.W. Rushforth, K.W. Edmonds, B.L. Gallagher, C.T. Foxon, J. Wunderlich, and T. Jungwirth, Tetragonal phase of epitaxial room-temperature antiferromagnet CuMnAs, *Nat. Commun.* 4 (2013) 2322.
- [5] L. Šmejkal, T. Jungwirth, and J. Sinova, Route towards Dirac and Weyl antiferromagnetic spintronics, *Phys. Status Solidi Rapid Res. Lett.* 11 (2017) 1700044.
- [6] P. Wadley, A. Crespi, J. Gázquez, M.A. Roldán, P. García, V. Novák, R. Champion, T. Jungwirth, C. Rinaldi, X. Martí, V. Holý, C. Frontera, and J. Rius, Obtaining the structure factors for an epitaxial film using Cu X-ray radiation, *J. Appl. Cryst.* 46 (2013) 1749.
- [7] V. Hills, P. Wadley, R.P. Champion, V. Novák, R. Beardsley, K.W. Edmonds, B.L. Gallagher, B. Ouladdiaf, and T. Jungwirth, Paramagnetic to antiferromagnetic transition in epitaxial tetragonal CuMnAs *J. Appl. Phys.* 117 (2015) 172608.
- [8] F. Máca, J. Kudrnovský, V. Drchal, K. Carva, P. Baláz, and I. Turek, Physical properties of the tetragonal CuMnAs: A first-principles study, *Phys. Rev. B* 96 (2017) 094406.
- [9] International Tables for Crystallography, Volume A: Space-group symmetry, edited by Theo Hahn, 5th ed., Kluwer Academic, Dordrecht, Boston, London, 2002.
- [10] G. Kresse and D. Joubert, From ultrasoft pseudopotentials to the projector augmented-wave method, *Phys. Rev. B* 59 (1999) 1758.
- [11] J.P. Perdew, K. Burke, and M. Ernzerhof, Generalized Gradient Approximation Made Simple, *Phys. Rev. Lett.* 78 (1997) 1396.
- [12] I. Turek, V. Drchal, J. Kudrnovský, M. Šob, and P. Weinberger, *Electronic Structure of Disordered Alloys, Surfaces and Interfaces*, Kluwer, Boston, 1997.
- [13] K. Carva, I. Turek, J. Kudrnovský, and O. Bengone, Disordered magnetic multilayers: Electron transport within the coherent potential approximation, *Phys. Rev. B* 73 (2006) 144421.
- [14] A.I. Liechtenstein, M.I. Katsnelson, V.P. Antropov, and V.A. Gubanov, Local spin density functional approach to the theory of exchange interactions in ferromagnetic metals and alloys, *J. Magn. Magn. Mater.* 67 (1987) 65.
- [15] I. Turek, J. Kudrnovský, V. Drchal, and P. Bruno, Exchange interactions, spin waves, and transition temperatures in itinerant magnets, *Philos. Mag.* 86 (2006) 1713.
- [16] K. Binder and D.W. Heermann, *Monte Carlo Simulation in Statistical Physics*, Springer, Berlin, 1997.
- [17] C. G. Van de Walle and J. Neugebauer, First-principles calculations for defects and impurities: Applications to III-nitrides, *J. Appl. Phys.* 95 (2004) 3851.
- [18] C. Frontera, private communication.
- [19] H. Ebert, S. Mankovsky, K. Chadova, S. Polesya, J. Minár, and D. Ködderitzsch, Calculating linear-response functions for finite temperatures on the basis of the alloy analogy model, *Phys. Rev. B* 91 (2015) 165132.
- [20] A.A. Starikov, Y. Liu, Z. Yuan, and P.J. Kelly, Calculating the transport properties of magnetic materials from first principles including thermal and alloy disorder, noncollinearity, and spin-orbit coupling, *Phys. Rev. B* 97 (2018) 214415.
- [21] B.L. Gyorffy, A.J. Pindor, J. Staunton, G.M. Stocks, and H. Winter, A first-principles theory of ferromagnetic phase transitions in metals, *J. Phys. F: Met. Phys.* 15 (1985) 1337.
- [22] J. Kudrnovský, V. Drchal, I. Turek, S. Khmelevskiy, J.K. Glasbrenner, and K.D. Belashchenko, Spin-disorder resistivity of ferromagnetic metals from first principles: The disordered-local-moment approach, *Phys. Rev. B* 86 (2012) 144423.
- [23] B. Skubic, J. Hellsvik, L. Nordström, and O. Eriksson, A method for atomistic spin dynamics simulations: implementation and examples, *J. Phys.: Condens. Matter* 20 (2008) 315203.
- [24] L. Bergqvist and A. Bergman, Realistic finite temperature simulations of magnetic systems using quantum statistics, *Phys. Rev. Mater.* 2 (2018) 013802.
- [25] K. Binder, Finite size scaling analysis of Ising model block distribution functions, *Z. Phys. B* 43 (1981) 119.